Journal of Power Sources 196 (2011) 7011–7015

Contents lists available at ScienceDirect

Journal of Power Sources

journal homepage: www.elsevier.com/locate/jpowsour

Short communication

Comparison between microparticles and nanostructured particles of $FeSn_2$ as anode materials for Li-ion batteries

Mohamad Chamas[a], Pierre-Emmanuel Lippens[a,*], Jean-Claude Jumas[a], Kada Boukerma[b], Rémi Dedryvère[b], Danielle Gonbeau[b], Jusef Hassoun[c], Stefania Panero[c], Bruno Scrosati[c]

[a] Institut Charles Gerhardt, Equipe Agrégats Interfaces et Matériaux pour l'Energie, Université Montpellier 2, Pl. E. Bataillon, 34095 Montpellier Cedex 5, France
[b] Institut Pluridisciplinaire de Recherche sur l'Environnement et les Matériaux, Equipe Chimie Physique, Université de Pau, 2 av. Pierre Angot, 64053 Pau Cedex 9, France
[c] Dipartemento di Chimica, Universita di Roma "La Sapienza", 00185 Rome, Italy

ARTICLE INFO

Article history:
Received 28 August 2010
Received in revised form
21 September 2010
Accepted 29 September 2010
Available online 7 October 2010

Keywords:
$FeSn_2$
Anodes
Li-ion
Mössbauer spectroscopy
Nanostructured material

ABSTRACT

The performances and mechanisms of two types of anodes formed by $FeSn_2$ microparticles and nanostructured $FeSn_2$, respectively, were studied by Mössbauer spectroscopy and electrochemical testing. The specific capacity, which is within the range 400–600 mAh g^{-1} even at high *C*-rate, did not vary with cycle number over 50–60 cycles for the microparticles but progressively decreased for the nanostructured material. In the two cases, the first discharge consists in the irreversible transformation of $FeSn_2$ into Fe/Li_7Sn_2 nanocomposite. The capacity fade is attributed to the growth and/or coalescence of the particles during cycling.

1. Introduction

Improvements in the energy density of Li-ion batteries require the development of new electrode materials with high specific capacity. This can be obtained for anode materials by moving from graphite (340 mAh g^{-1}) to metals that form alloys with lithium such as silicon (4200 mAh g^{-1}) or tin (990 mAh g^{-1}). However, such alloying reactions are associated to large volume variations that lead to loss of electrical contacts during cycling and capacity fade. In order to improve the cycle life, M–Sn and M–Sn–C materials, where M is a transition metal, have been proposed [1–5]. The electrochemically inactive metallic particles M, extruded during the first lithiation, are expected to buffer the volume variations and to limit the growth and coalescence of tin based particles during the electrochemical cycling. In addition, the electrochemical performances are often found to be improved by the use of small M–Sn particles. But this also increases the reactivity of the particles with electrolyte and the irreversible capacity of the first discharge. Thus, it is still interesting to compare the performances of microsized and nanosized particles.

Cobalt is certainly one of the most studied transition metals. It has been used with Sn and C to form nanostructured alloys as commercialized by Sony in 2005 [6] and seems to be the best candidate for the Sn–M–C composites [7]. In order to reduce the cost of the electrode materials, the partial substitution of Co by Fe has been proposed recently [8] and it should be interesting to reconsider iron–tin based anodes. The most tin rich binary phase, $FeSn_2$, was studied in the past as possible nanostructured anode material for Li-ion batteries [9] but to our knowledge there is no published study on $FeSn_2$ microparticles obtained by ceramic route. In the present study, we compare the specific capacities of both $FeSn_2$ microparticles and nanostructured materials at different *C*-rates. Mössbauer spectroscopy was used to characterize the electrode at the end of the first discharge which is an essential step in the restructuration of the pristine electrode. This technique is also used to relate the observed capacity fade to changes in the particle morphology during cycling.

2. Experimental

The $FeSn_2$ microparticles were prepared directly from pure elements: micrometric Sn (Sigma–Aldrich, 99.5% purity) and Fe (Sigma–Aldrich, 99.5% purity) in an alumina crucible under controlled Ar/H_2 (5%) atmosphere, heated at 470 °C for 5 h before air-quenched. The $FeSn_2$ nanostructured particles were obtained

* Corresponding author. Tel.: +33 4 67 14 45 48; fax: +33 4 67 14 33 41.
E-mail address: lippens@univ-montp2.fr (P.-E. Lippens).

0378-7753/$ – see front matter © 2010 Elsevier B.V. All rights reserved.
doi:10.1016/j.jpowsour.2010.09.113

by ball milling from the $FeSn_2$ microparticles (Retsch PM 100) with stainless steel balls and grinding jars. A powder charge of 3 g was milled with five balls of 5 g each for 72 h but stopped every 15 min active milling during 15 min for the cooling of the powder. The purity and the crystallinity of the powder materials were controlled by X-ray diffraction (XRD) with a PHILIPS X'Pert MPD equipped with the X'celerator detector. The XRD patterns were recorded using Cu Kα radiation (λ = 1.5418 Å). The morphology of the samples was characterized by scanning electron microscopy (SEM).

Electrochemical tests were carried out with Swagelok™-type two-electrode cells assembled inside an argon-filled glove box. A lithium foil was used as counter electrode. The working electrode was made up of 80 wt.% pristine material, 10 wt.% polymer binder, and 10 wt.% carbon black (SP) as conductive additive, and deposed on cupper film by a doctor blade. Polyvinylidene fluoride (PVDF) was used as binder for electrochemical tests, while polytetrafluoroethylene (PTFE) was used for XPS characterization. For Mössbauer measurements, a PTFE based composite was pressed into pellets (7 mm diameter). The electrolyte was composed of 1 M $LiPF_6$ with ethylene carbonate (EC) and dimethyl carbonate (DMC), EC:DMC 1:1. A glass microfiber paper (Whatman) was used as separator. Electrochemical discharge/charge curves were recorded on a Maccor Series 4000 Battery test system (or multichannel Mac Pile II system for Mössbauer measurements) under galvanostatic conditions at different *C*-rate regimes: *C*/50-1*C* (1*C* corresponds to a full first discharge of the cell in 1 h) between 0.01 and 1.2 V vs. Li^+/Li^0.

XPS measurements were carried out with a Kratos Axis Ultra spectrometer using a focused monochromatized Al Kα radiation ($h\nu$ = 1486.6 eV). For the Ag $3d_{5/2}$ line, the full width at half maximum was 0.58 eV under the recording conditions. The binding energy scale was calibrated from the carbon contamination using the C 1s peak at 285.0 eV. Core peaks were analyzed using a nonlinear Shirley-type background. The peak positions and areas were optimized by a weighted least-square fitting method using 70% Gaussian, 30% Lorentzian lineshapes.

^{119}Sn and ^{57}Fe Mössbauer spectra were recorded in transmission geometry and constant accelerator mode at room temperature with ^{119m}Sn in a $CaSnO_3$ matrix and $^{57}Co(Rh)$ as sources, respectively. In the two cases, the velocity scale was calibrated using the magnetic six-line spectrum of a high-purity iron foil absorber as a standard and using $^{57}Co(Rh)$ as the source. The hyperfine parameters were determined with a non-linear least-square method, by using the program GM5SIT [10] and the Lorentzian profiles. The isomer shifts are given with respect to $BaSnO_3$ and α-Fe for the ^{119}Sn and ^{57}Fe Mössbauer measurements, respectively.

3. Results and discussion

The XRD patterns show that both microparticles and nanostructured materials have good crystallinity and high purity. All the diffraction peaks can be assigned to $FeSn_2$ (Fig. 1). The average sizes of the secondary particles were roughly evaluated from SEM to several micrometers and several hundred nanometers, for microparticles and nanostructured particles, respectively (Fig. 2). The two types of $FeSn_2$ particles can be easily distinguished from their ^{119}Sn Mössbauer spectra at room temperature (Fig. 3). The observed differences are due to the antiferromagnetic [11] and superparamagnetic [12] properties of the microparticles and nanostructured particles, respectively. The hyperfine parameters obtained from the spectra (Table 1) are in good agreement with previously published values, which confirms the purity of the materials.

The specific capacity of the first discharge is of about 800 mAh g^{-1} for the microparticles at all the *C*-rates considered in the present study and rise up to more than 1000 mAh g^{-1} for the nanostructured materials at low *C*-rates. In all the cases, there is a large irreversible capacity loss between the first discharge and the first charge leading to a reversible capacity in the range of 400–600 mAh g^{-1}. At high *C*-rates (*C*/5-*C*), the specific capacity of

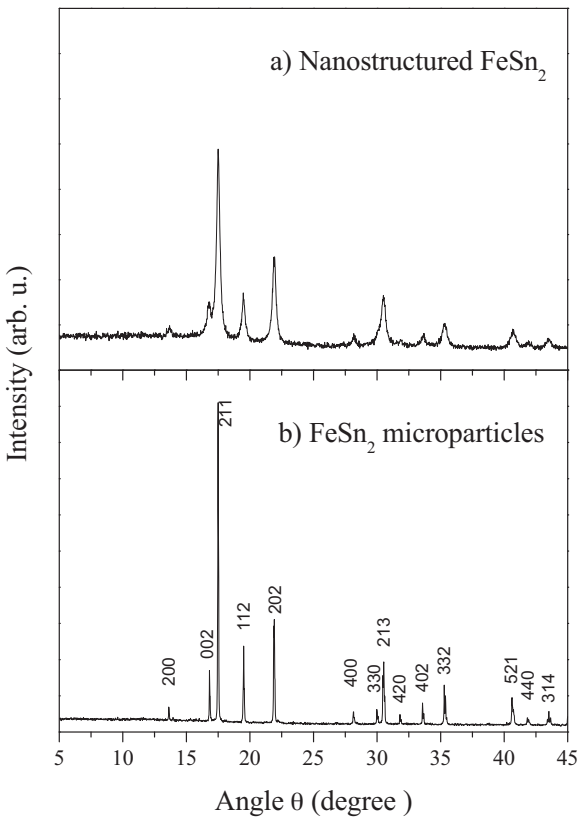

Fig. 1. XRD patterns of nanostructured $FeSn_2$ (a) and $FeSn_2$ microparticles (b).

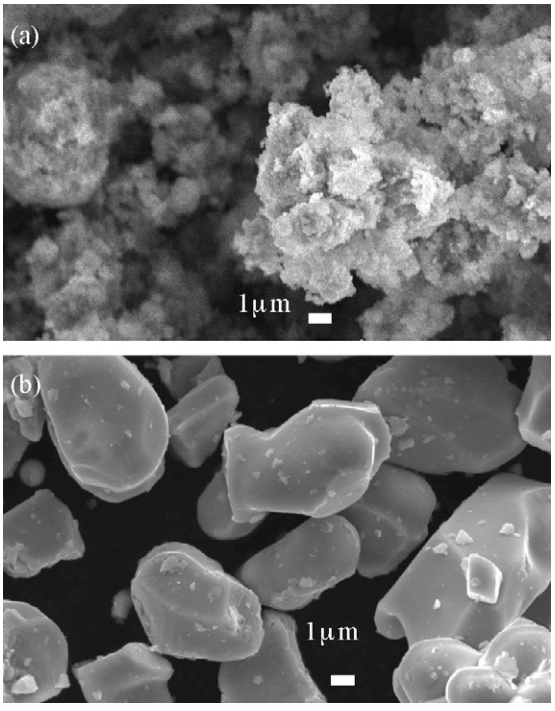

Fig. 2. SEM images of nanostructured $FeSn_2$ (a) and $FeSn_2$ microparticles (b). Scale: 1 μm (horizontal bar).

Table 1
^{119}Sn and ^{57}Fe Mössbauer parameters for $FeSn_2$ powders and electrode materials: isomer shift (δ), quadrupole splitting (Δ), magnetic hyperfine field (H), linewidth (Γ) and relative contribution (RC). The ^{119}Sn and ^{57}Fe isomer shifts are given with respect to $BaSnO_3$ and α-Fe, respectively. The two ^{119}Sn components of the spectra at the end of discharge are labeled by the Sn site symmetry within Li_7Sn_2 while those of ^{57}Fe denote superparamagnetic (1) and ferromagnetic (2) components.

	Site		δ (mm s^{-1})	Δ (mm s^{-1})	H (T)	Γ (mm s^{-1})	RC (%)
$FeSn_2$ microparticles	^{119}Sn		2.18	0.83	2.4	0.89	100
Nanostructured $FeSn_2$	^{119}Sn		2.20	0.9	–	0.94	100
Electrode-$FeSn_2$ microparticles	^{119}Sn	4*i*	1.88	0.23	–	0.99	50
End of 1st discharge		4*h*	1.98	0.72	–	0.99	50
Electrode-nanostructured $FeSn_2$	^{119}Sn	4*i*	1.88	0.17	–	0.96	50
End of 1st discharge		4*h*	1.96	0.68	–	0.96	50
Electrode-$FeSn_2$ microparticles	^{119}Sn	4*i*	1.92	0.29	–	0.98	50
End of 30th discharge		4*h*	2.00	1.08	–	0.98	50
	^{57}Fe	1	0.22	0	0	0.99	53
		2	0.16	0	32.6	0.88	47

the microparticles is almost constant until about 50–55 cycles and then decreases, while it continuously decreases for the nanostructured particles as shown in Fig. 4 for the 1*C* rate. Such capacity retention was obtained at 1*C* after a first discharge at *C*/10 as activation process because using initial high *C*-rate leads to a progressive increase of the specific capacity for the first 10 cycles (Fig. 5). This shows that first discharge is of real importance in the electrochemical behavior of intermetallic compounds. At lower *C*-rate such an activation step was not necessary to stabilize the capacity. The comparison with βSn nanoparticles clearly indicates the positive role of iron on capacity fade (Fig. 4). This is usually attributed to the formation of metallic nanoparticles during the first discharge of intermetallic compounds (conversion reaction). These metallic particles are electrochemically inactive and are expected to mechanically buffer volume variations during the electrochemical reaction of lithium with tin after the first discharge. Similar performances were obtained at *C*/5 and *C*/10. Only a small decrease in the specific capacity and a poorer capacity retention were observed at lower *C*-rates (<*C*/10). Thus, for both microparticles and nanostructured materials and at all the *C*-rates studied here (*C*/50-1*C*), there is a significant decrease of the specific capacity after about 50 cycles. Such a behavior was also observed for Fe–Sn–C composites [5].

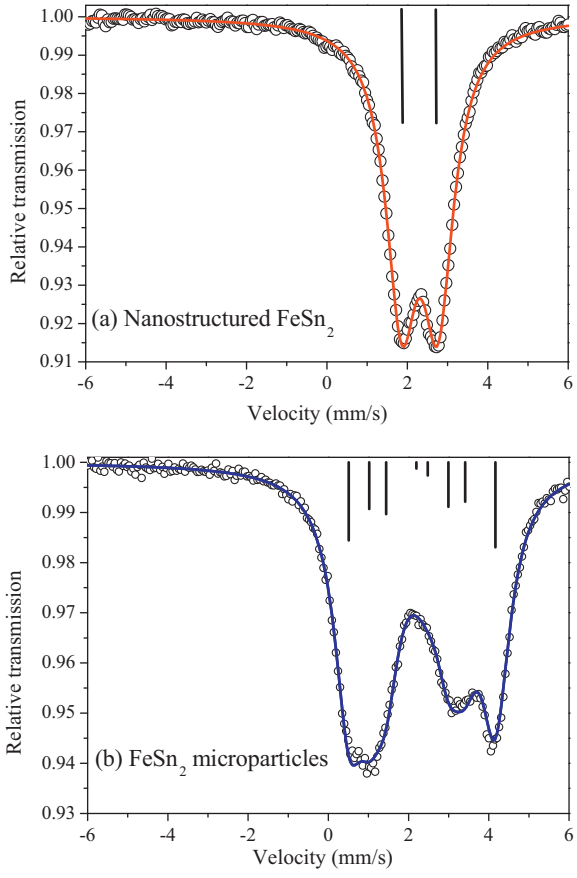

Fig. 3. ^{119}Sn Mössbauer spectra at room temperature of nanostructured $FeSn_2$ (a) and $FeSn_2$ microparticles (b).

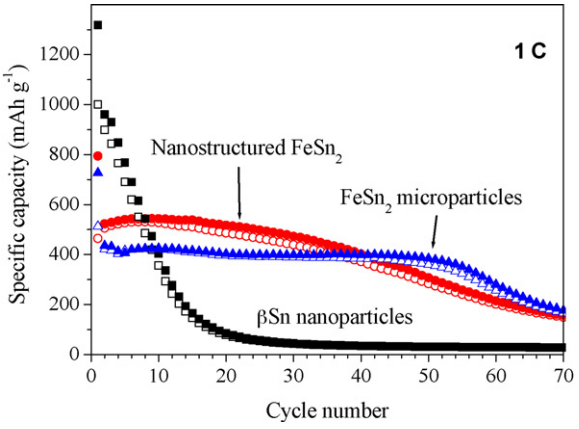

Fig. 4. Specific capacities of nanostructured $FeSn_2$ (circles), $FeSn_2$ microparticles (triangles) and βSn nanoparticles (squares) as a function of the cycle number at 1*C* rate. The full and empty symbols denote the discharges and charges, respectively.

The main differences between the voltage profiles of microparticles and nanostructured materials, obtained at low lithium rates, concern the first discharge (Fig. 6). In the two cases, the potential

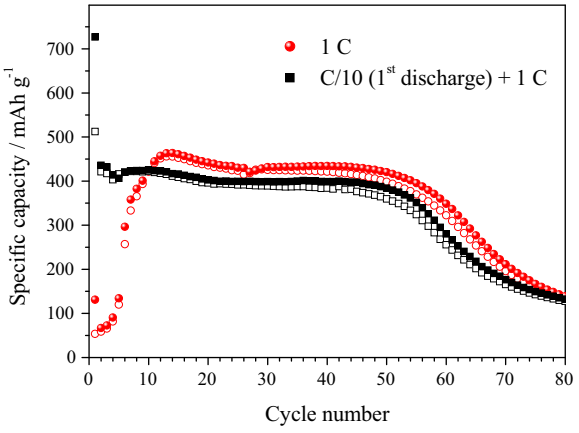

Fig. 5. Specific capacities of $FeSn_2$ microparticles based electrodes as a function of the cycle number at 1*C* rate without (circles) and with (squares) a first discharge at *C*/10 rate. The full and empty symbols denote the discharges and charges, respectively.

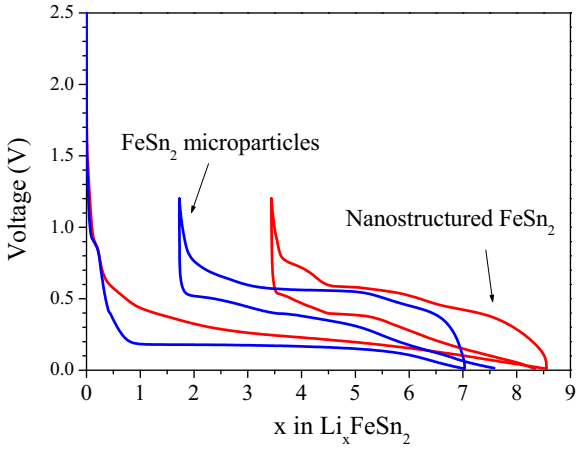

Fig. 6. Voltage (vs. Li^+/Li) profiles of $FeSn_2$ based electrodes at *C*/50.

curves show a small plateau at about 0.9 V due to the formation of the solid electrolyte interphase (SEI) at the surface of the carbonated additive surface. Then, for the microparticles, the potential decreases until the reaction of about 1 Li and forms a well defined plateau at about 0.2 V until 6 Li and then drops to 0 V at the end of discharge (≈7 Li). For the nanostructured particles there is a continuous decrease of the potential until the end of discharge at about 8.5 Li. No changes were observed in the experimental data obtained by XRD and Mössbauer spectroscopy at the beginning of the discharge (<1 Li for microparticles and 1.5 Li for nanostructured particles) suggesting that $FeSn_2$ did not react with lithium. This is confirmed by XPS spectra recorded after reaction with 0.5 and 1 Li. Indeed, they display a strong decrease of the signals of the $FeSn_2$ material (Sn 3d peak) and of the carbon black (C 1s peak) resulting from the covering process of the electrode by the SEI film. This shows that all the lithium at the very beginning of discharge has been consumed to form the surface film. An example of C 1s spectrum obtained for the $FeSn_2$ electrode (microparticles) after reaction with 1 Li is given in Fig. 7. It shows a weak C 1s component at 283 eV assigned to carbon black, whereas it is the main component of the pristine electrode. The C 1s peak of the PTFE binder (CF_2) at 292.5 eV is still well observable since it was not covered by the SEI. Four additional

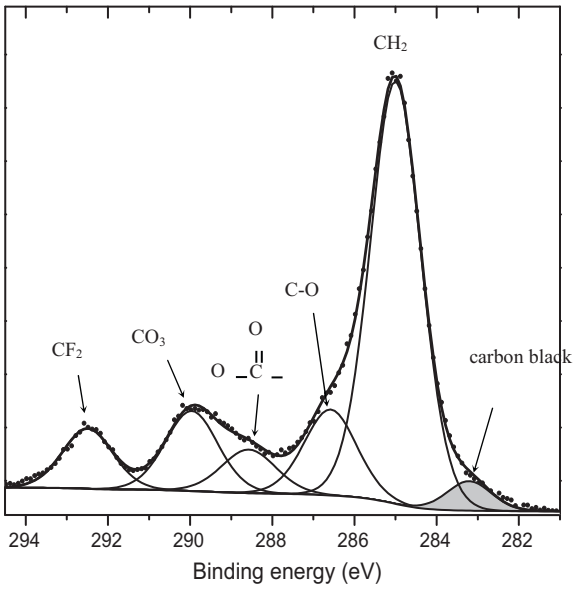

Fig. 7. XPS C 1s spectrum of the $FeSn_2$ electrode (microparticles) after reaction with one lithium ($x = 1$) upon the first discharge of a $FeSn_2$/Li cell.

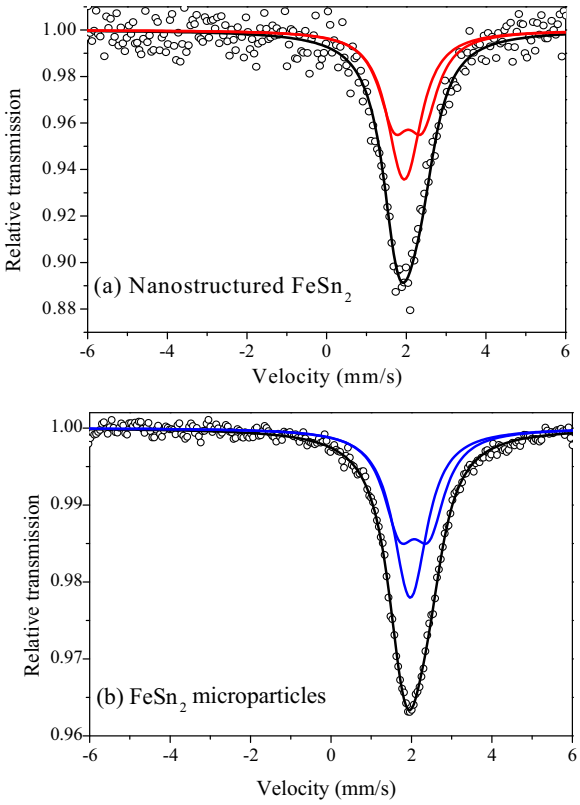

Fig. 8. ^{119}Sn Mössbauer spectra at room temperature of nanostructured $FeSn_2$ (a) and $FeSn_2$ microparticles (b) based electrodes, at the end of the first discharge.

components at 285, 286.5, 288.5 and 290 eV are observed after discharge, corresponding to carbon atoms in CH_2, C–O, O=C–O and CO_3-like environments, respectively. They display the formation of carbonaceous species making up the SEI, resulting from the degradation of the electrolyte's solvents at the surface of the electrode. Several mechanisms can be found elsewhere [13]. Similar C 1s spectra were observed after further discharge, and are also similar to C 1s spectra recorded with other tin-based intermetallics such as Cu_6Sn_5 [14] or Ni_3Sn_4 [15].

After the SEI formation, both XRD patterns and Mössbauser spectra show changes that can be attributed to the transformation of $FeSn_2$ into Li–Sn alloys. As previously observed for other tin intermetallic compounds it is difficult to determine the composition of the fully lithiated products from this technique because of the small size and/or the poor crystallinity of the particles. In this case, atomic-scale characterization tools such as Mössbauer spectroscopy are of great help [15,16]. At the end of discharge, the ^{119}Sn Mössbauer spectra obtained for both $FeSn_2$ microparticles and nanostructured materials are very similar (Fig. 8). The hyperfine parameters (Table 1) are close to those obtained at the end of the discharge of other tin intermetallic compounds and can be assigned to Li_7Sn_2 [16,17]. It is worth noting that values of one of the highest quadrupole splitting differ from those of bulk Li_7Sn_2 [18]. This can be explained by differences in the Sn local environments due to the small size and/or the poor crystallinity of the Li_7Sn_2 particles formed within the electrode. Thus, for the two types of pristine materials, the first discharge consists in the transformation of $FeSn_2$ into a Fe/Li_7Sn_2 nanocomposite. The observed differences in the shape of the potential curves cannot be attributed to strong differences in the electrode restructuration mechanisms but could be due to interface reactions, which are more important in nanostructured materials, or to differences in kinetic effects that are related to particle size or morphology. The additional 1.5 Li involved in the

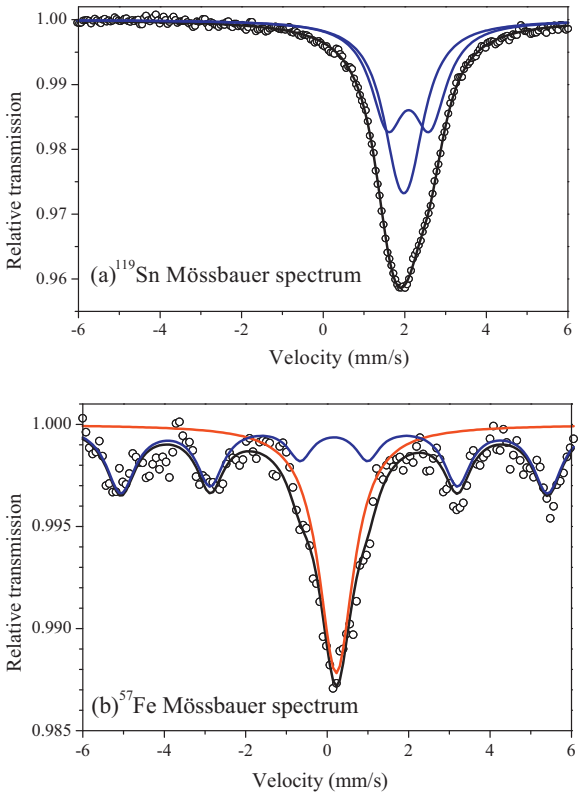

Fig. 9. ^{119}Sn (a) and ^{57}Fe (b) Mössbauer spectra at room temperature of the $FeSn_2$ microparticles based electrode at the end of the 30th discharge.

first discharge of nanostructured particles could be due to these effects and to a small amount of unreacted $FeSn_2$ microparticles that cannot be detected by Mössbauer spectroscopy.

The charge process is more complex and will be described in details for the microparticles elsewhere. But since similar Fe/Li_7Sn_2 nanocomposites were obtained at the end of the first discharge for the two types of electrodes, a simple qualitative explanation can be proposed based on the previously published mechanisms for nanostructured particles [9]. The first charge can be considered as a progressive delithiation of Li_7Sn_2 and a back reaction of poorly lithiated Li–Sn phases with the iron nanoparticles obtained at the end of the first discharge. The second discharge leads to the reformation of the Fe/Li_7Sn_2 nanocomposite as observed from Mössbauer spectroscopy. The following electrochemical cycles are similar to the 1st charge/2nd discharge cycle confirming that the first discharge is an irreversible restructuring step. The nanocomposite obtained at the end of the first discharge should be considered as the real electrode material for electrochemical cycling.

After 30 cycles, the ^{119}Sn Mössbauer spectrum obtained at the end of discharge shows the typical asymmetrical shape of bulk Li_7Sn_2 (Fig. 9a) as confirmed by the values of the hyperfine parameters (Table 1). The ^{57}Fe Mössbauer spectrum shows a magnetic sextet and was fitted with two components (Fig. 9b). The values of the hyperfine parameters for the sextet component (Table 1) are close to those of α-Fe bulk material while the other component can be attributed to superparamagnetic iron nanoparticles. Thus, both ^{119}Sn and ^{57}Fe Mössbauer data show the existence of large Li_7Sn_2 and Fe particles that can be attributed to the growth and/or coalescence of the particles during cycling. This effect is here clearly evidenced by Mössbauer spectroscopy and explains the capacity fade. Indeed, large particles decrease the efficiency of electrochemical reactions compared to nanoparticles but the main effect is the loss of electrical contacts due to stronger volume changes. In the present work, the variations of the specific capacity vs. cycle number suggest that this effect is progressive for nanostructured particles while it occurs after a certain number of cycles for microparticles. Since in the two cases the electrochemical reactions are very similar, this could be due to differences in the evolution of the electrode material morphology during cycling.

4. Conclusion

$FeSn_2$ microparticles and nanostructured particles have been investigated as anode materials for Li-ion batteries. In the two cases the first discharge is based on the transformation of $FeSn_2$ into Fe/Li_7Sn_2 nanocomposite. This irreversible conversion reaction is an important restructuration step of the pristine electrode which should be performed at a low *C*-rate. The Fe/Li_7Sn_2 nanocomposite can be considered as the real starting material for the reversible lithiation/delithiation reactions during cycling. The specific capacity of $FeSn_2$ based electrodes is higher than that of carbon based electrodes, even at 1*C* rate, but is retained over 50 cycles. The capacity fade is mainly due to the growth and/or coalescence of the particles during cycling. The observed differences in the specific capacity vs. cycle number between microsized and nanostructured pristine materials could be due to the morphology of the particles which influences the mechanical and electrical properties of the $FeSn_2$/binder/conductive additive composites.

Acknowledgement

This work has been carried out in the framework of the European Research Institute ALISTORE.

References

[1] M.M. Thackeray, J.T. Vaughey, A.J. Kahaian, K.D. Kepler, R. Benedek, Electrochem. Commun. 1 (1999) 111.
[2] D. Larcher, L.Y. Beaulieu, D.D. MacNeil, J.R. Dahn, J. Electrochem. Soc. 147 (2000) 1658.
[3] J. Hassoun, S. Panero, B. Scrosati, J. Power Sources 160 (2006) 1326.
[4] J. Hassoun, S. Panero, G. Mulas, B. Scrosati, J. Power Sources 171 (928) (2007) 928.
[5] P.P. Ferguson, M.L. Martine, A.E. George, J.R. Dahn, J. Power Sources 194 (2009) 794.
[6] H. Tanizaki, A. Omaru, US Patent 0,053,131 A1 (2004), to Sony Corporation.
[7] A.D.W. Todd, R.E. Mar, J.R. Dahn, J. Electrochem. Soc. 153 (2006) A1998.
[8] P.P. Ferguson, R.A. Peng Liao, J.R. Dunlap, Dahn, J. Electrochem. Soc. 156 (2009) A13.
[9] R.A. Dunlap, O. Mao, J.R. Dahn, Phys. Rev. B 59 (1999) 3494.
[10] K. Ruebenbauer, T. Birchall, Hyperfine Interact 7 (1979) 125.
[11] G. Le Caër, B. Malaman, G. Venturini, D. Fruchart, B. Roques, J. Phys. F 15 (1985) 1813.
[12] O. Mao, R.A. Dunlap, I.A. Courtney, J.R. Dahn, J. Electrochem. Soc. 145 (1998) 4195.
[13] K.K.D. Ehinon, S. Naille, R. Dedryvère, P.-E. Lippens, J.-C. Jumas, D. Gonbeau, Chem. Mater. 20 (2008) 5388.
[14] S. Naille, R. Dedryvère, H. Martinez, S. Leroy, P.-E. Lippens, J.-C. Jumas, D. Gonbeau, J. Power Sources 174 (2007) 1086.
[15] S. Naille, R. Dedryvère, D. Zitoun, P.-E. Lippens, J. Power Sources 189 (2009) 806.
[16] C.-M. Ionica-Bousquet, P.-E. Lippens, L. Aldon, J. Olivier-Fourcade, J.-C. Jumas, Chem. Mater. 18 (2006) 6442.
[17] S. Naille, C.M. Ionica-Bousquet, F. Robert, F. Morato, P.-E. Lippens, J. Olivier-Fourcade, J. Power Sources 174 (2007) 1091.
[18] F. Robert, P.-E. Lippens, J. Olivier-Fourcade, J.-C. Jumas, F. Gillot, M. Morcrette, J.-M. Tarascon, J. Solid State Chem. 180 (2007) 339.